Title	High rate lithium ion cycling in electrodeposited binder-free thin film vanadium oxide cathodes with lithium metal anodes in ionic liquid and polymer gel analogue electrolytes
Authors	McGrath, Louise M.;Rohan, James F.
Publication date	2020-11-05
Original Citation	McGrath, L. M. and Rohan, J. F. (2020) 'High rate lithium ion cycling in electrodeposited binder-free thin film vanadium oxide cathodes with lithium metal anodes in ionic liquid and polymer gel analogue electrolytes', Batteries & Supercaps. doi: 10.1002/batt.202000236
Type of publication	Article (peer-reviewed)
Link to publisher's version	10.1002/batt.202000236
Rights	© 2020, WILEY#VCH Verlag GmbH & Co. This is the peer reviewed version of the following article: McGrath, L. M. and Rohan, J. (2020) 'High rate lithium ion cycling in electrodeposited binder-free thin film vanadium oxide cathodes with lithium metal anodes in ionic liquid and polymer gel analogue electrolytes', Batteries & Supercaps, doi: 10.1002/batt.202000236, which has been published in final form at https://doi.org/10.1002/batt.202000236. This article may be used for non-commercial purposes in accordance with Wiley Terms and Conditions for Use of Self-Archived Versions.
Download date	2025-01-07 01:43:56
Item downloaded from	https://hdl.handle.net/10468/10757

University College Cork, Ireland
Coláiste na hOllscoile Corcaigh

Batteries & Supercaps

Chemistry Europe
European Chemical Societies Publishing

Accepted Article

Title: High rate lithium ion cycling in electrodeposited binder-free thin film vanadium oxide cathodes with lithium metal anodes in ionic liquid and polymer gel analogue electrolytes

Authors: Louise M. McGrath and James Rohan

To be cited as: *Batteries & Supercaps* 10.1002/batt.202000236

Link to VoR: https://doi.org/10.1002/batt.202000236

WILEY-VCH

10.1002/batt.202000236

WILEY-VCH

ARTICLE

High rate lithium ion cycling in electrodeposited binder-free thin film vanadium oxide cathodes with lithium metal anodes in ionic liquid and polymer gel analogue electrolytes

L. M. McGrath,[a] J. F. Rohan[a]*

[a] L. M. McGrath and Dr. J. F. Rohan
Electrochemical Materials and Energy Group
Tyndall National Institute
University College Cork
Lee Maltings
T12 R5CP
Cork
Ireland
E-mail: james.rohan@tyndall.ie

Abstract: High rate and long cycle life performance for electrodeposited, binder-free V_2O_5 thin film cathodes and lithium metal anodes is described using liquid and polymer gel electrolytes of the pyrrolidinium based (C_4mpyrTFSI) ionic liquid (IL). Sharp well-defined voltammetric peaks typically seen with nanostructured V_2O_5 materials in organic electrolytes, support the fast kinetics observed. The addition of vinylene carbonate (VC) stabilises the electrolyte interface leading to higher electrode capacities than for the additive-free electrolyte, ~ 120 versus ~90 mAh g^{-1} at 0.75 C. Polymer gel electrolytes based on the IL yield similar electrode capacities, coulombic efficiencies and high rate performances without the VC-additive. The polymer gel option delivers the better long-term stability up to 400 cycles with lithium metal anodes with minimal capacity fade at elevated charge and discharge rates up to 5 C.

Introduction

The conceptualisation of the Internet of Things (IoT), has led to an increased demand for miniaturised IoT sensors.[1] In order to ensure autonomy, energy harvesters coupled with appropriate energy storage systems are necessary. Typical Li microbatteries utilise lithium cobalt oxide ($LiCoO_2$) cathode coupled with Li metal and a solid-state electrolyte. However, cobalt (Co) is not an abundant material and can only be mined in a small number of global locations where the largest share (~50%) is found in the Democratic Republic of Congo.[2] This has led to price instability and a dramatic increase from ~$21,000 per metric tonne in January of 2016 to $95,307 in March of 2018, and more recently $34,500 in February 2020.[3] Therefore researchers are investigating cathode materials with decreased Co content or ultimately entirely Co-free.

Vanadium pentoxide (V_2O_5), is of particular interest due to lower cost, wider availability and higher energy density. V_2O_5 thin films can be prepared by various deposition techniques such as including sol-gel [4], spray pyrolysis[5], thermal evaporation[6], electron beam evaporation[7], pulsed laser deposition[7a, 8], chemical vapour deposition[9], ion beam sputtering[10], electrodeposition[11] and D.C.[12] or R.F. sputtering[12b, 13]. Electrodeposition is a well-established and relatively low-cost option that is scalable to produce uniform deposits. Fabrication of thin films through electrodeposition can facilitate sequential layer build-up processes typically used in microbatteries.

Typically V_2O_5 analysis for Li based battery applications has been carried out in organic-based electrolytes,[14] however, being liquids with high volatility hinders their use in thin film microbatteries. Typical solid-state electrolytes such as LiPON have low ionic conductivities, typically 3 x10^{-3} mS cm^{-1},[15] which often result in low rate capabilities. Therefore, we assessed the electrochemical performance of V_2O_5 with an IL and subsequently polymer analogue electrolyte, whose favourable properties, high ionic conductivity and non-volatility, offer a compromise between solid-state and organic electrolytes. Chou *et al.*[16] described the

10.1002/batt.202000236

electrochemical performance of specifically nanostructured V_2O_5 morphologies with 1-propyl-1-methyl-pyrrolidinium bis(trifluoromethylsulfonyl)imide (C_3mpyrTFSI) electrolyte. The results from that study showed an improved electrochemical performance of V_2O_5 in the IL when compared to a conventional organic electrolyte (1 M $LiPF_6$ in EC/DMC (1:1)). The electrochemical analysis described in this work utilised 1-butyl-1-methylpyrrolidinium bis(trifluoromethylsulfonyl)imide (C_4mpyrTFSI) based electrolytes. The combination of plated thin film V_2O_5 and C_4mpyrTFSI-based electrolytes is shown to facilitate long-term cycling with metallic Li anodes surpassing the 20 to 100 cycles typically reported.[17] In this study, the stability of V_2O_5 in the ionic liquid was investigated using cyclic voltammetry (CV) and galvanostatic cycling to determine the cycling efficiency and electrode capacity including long term cycling at elevated C-rates. The initial analysis is focused on determining whether crystalline or amorphous films are better suited for Li^+ cycling with C_4mpyrTFSI as some amorphous oxide materials such as TiO_2 have been reported to exhibit better electrochemical performance than their crystalline counterparts.[18] We utilised carbonate additives in the butyl-methylpyrrolidinium-based ILs to investigate if it suppresses the growth of Li dendrites to enable enhanced cycle life with metallic lithium anodes as previously reported for typical organic-based electrolytes. [19] The use of VC is also investigated to develop a more stable cathode electrolyte interface (CEI) layer at the V_2O_5. Finally, long-term cycling analysis is shown up to 400 cycles with increasing C-rates, such as 50 cycles at 5 C, with both the IL and polymer gel electrolytes to determine the long-term stability of the V_2O_5/Li metal cell.

Results and Discussion

Electrodeposition was used to obtain porous V_2O_5 thin films with similar film morphologies to those previously described in the literature (figure 1(a)).[11a] SEM analysis indicates a crystallite size of approximately 130 nm (inset figure 1b). EDX analysis confirms a V:O ratio of 5:2 which matches the compositions reported in the literature.[20] The crystal structures of V_2O_5 in the local environment and x-z projection, are shown in figure 1(c) and (d) respectively. The as-deposited films shown in figure 1(e) yielded broad, low-intensity peaks, which is indicative of an amorphous film.[21] The peak assignments at 200 and 450 cm^{-1} are attributed to the bending vibration modes of the V_3-O (triply co-ordinated oxygen), V_2-O (doubly co-ordinated oxygen) and V=O (terminal) bonds in a disordered V-O-V framework, while the peak at 520 cm^{-1} is due to the stretching vibration modes of the V_3-O bonds in a disordered V-O-V framework.

Annealing the electrodeposited V_2O_5 at 325 ºC yielded crystalline films confirmed by Raman spectroscopy with intense, sharp well-defined peaks as shown in figure 1(d), which match the literature data for the orthorhombic phase of V_2O_5,[11e, 21a, 21b, 21e]. The orthorhombic phase of V_2O_5 has a well-established spectrum with a space group *Pmmn* and D_{2h} point symmetry.[22] There are 4 symmetry equivalent atomic positions per unit cell, and 12 symmetrical combinations can be built from the Cartesian displacement of the equivalent atoms. Six of the combinations are IR-active and six are Raman active. A_g and B_{2g} Raman modes are from the displacements of the x and z-axis while the B_{1g} and B_{3g} Raman modes come from displacement of the y-axis. In some symmetries, half the bond length is shortening, and the other half is stretching so the bond stretching and shortening cancel each other out. The peaks for the annealed films correspond to in-phase stretching vibration of V=O1 bonds (993.40 cm^{-1}), anti-phase stretching of V-O2 bonds (700.90 cm^{-1}), x-axis displacements of stretching O2 atoms (524.9 cm^{-1}), bending of V-O3-V bridge angle (482.30 cm^{-1}), x-axis displacement of O1 atoms (403.70 cm^{-1}), z-axis displacements of $O2_1$ and $O2_2$ atoms (302.60 cm^{-1}), y-axis displacement of O1 atoms (283.20 cm^{-1}),

10.1002/batt.202000236

ARTICLE

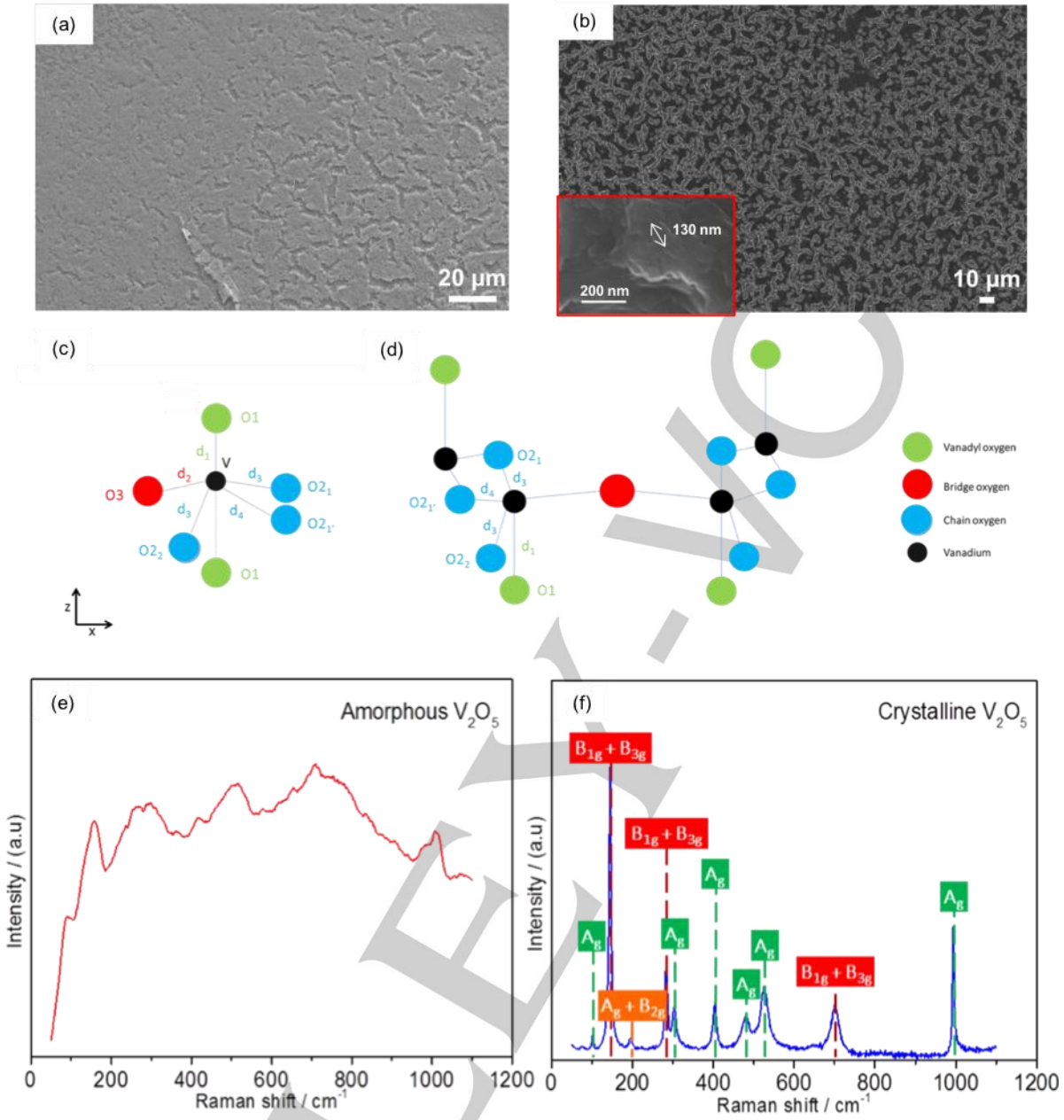

Figure 1: SEM analysis of (a) amorphous and (b) crystalline V_2O_5 thin films (inset indicates crystallite size), where EDX analysis determined a 5:2 V:O ratio. Crystal structure of V_2O_5 in the (c) local environment and (d) x-z projection. Raman spectra of (e) amorphous V_2O_5 and (f) crystalline V_2O_5 with peak assignments. Figure 1(c and d) adapted with permission from Baddour-Hadjean et al.[22a] Copyright 2020 American Chemical Society

x-axis displacement of V atoms (195.10 cm^{-1}), V atoms mixed signal of shear motion and rotation of the ladders, and O3-V-O2, in the y-axis (144.70 cm^{-1}), and V atom vibration in the O3-V-O2 bridge in the z-axis (103 cm^{-1}). The peaks at 195.10 cm^{-1} and 144.70 cm^{-1} correspond to the lattice vibration and are strongly associated with a layered structure.[21d, 23] Based on the Raman spectra, the unannealed V_2O_5 thin films are amorphous with a disordered framework, while the annealed V_2O_5 thin films are crystalline with a layered structure as evidenced by the peak assignments. In addition, the Raman analysis did not detect

10.1002/batt.202000236

ARTICLE

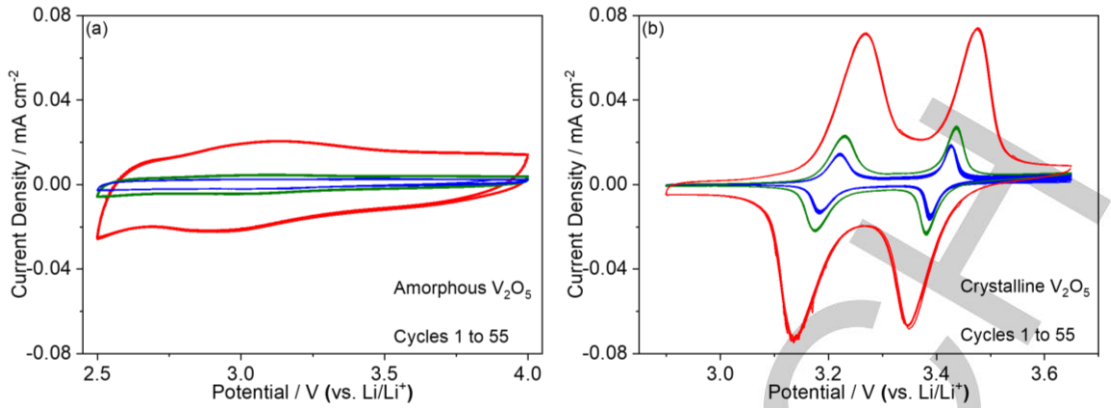

Figure 2: CV comparison of (a) amorphous and (b) crystalline V_2O_5 thin film electrodes in 0.5 M LiTFSI in C_4mpyrTFSI. Scan rates: 0.05 mV s^{-1} (blue), 0.1 mV s^{-1} (green) and 0.5 mV s^{-1} (red)

peaks associated with VO_2 indicating that any tetravalent vanadium present is a very small percentage which is in agreement with other studies reported in the literature.[21e, 24]

The electrodeposition of V_2O_5 produces thin films compatible with microbattery fabrication processes. Typically, a solid-state electrolyte is utilised to facilitate sequential layer build-up, however, as V_2O_5 thin films with C_4mpyrTFSI electrolytes have not been previously reported, the initial analysis was carried out with liquid electrolytes followed by the solid-state polymer gel analogue. Distinct differences between the electrochemical performance of amorphous and crystalline V_2O_5 films have been previously observed for lithium based batteries in organic electrolytes.[21a, 25] CV analysis for both amorphous and crystalline electrodeposited V_2O_5 electrodes is shown in figure 2. Amorphous materials lack long-range order or required ion diffusion channels leading to isotropic lithium diffusion.[26] This results in the broad peaks observed in figure 2(a), indicative of pseudo-capacitive storage, either at the particle surface or within the interlayer spacing of the material.[21a, 25b] To get appreciable capacities the cycling must be conducted over the potential range 2.5 to 4.0 V. In contrast, sharp very well-defined peaks are observed for the crystalline material over a potential range of 2.9 to 3.6 V as shown in equations 1 to 3.[27]

$$V_2O_5 + xLi + xe^- \leftrightarrow \alpha Li_xV_2O_5 \quad (x < 0.1) \qquad \text{Equation 1}$$

$$V_2O_5 + xLi + xe^- \leftrightarrow \varepsilon Li_xV_2O_5 \quad (0.35 < x < 0.7) \qquad \text{Equation 2}$$

$$V_2O_5 + xLi + xe^- \leftrightarrow \delta Li_xV_2O_5 \quad (x = 1) \qquad \text{Equation 3}$$

Equations 1 and 2 refer to peaks that occur at ~3.3 V and ~3.4 V, as these peaks correspond to α/ε transitions, while ε/δ transition peaks at ~3.1 V and ~3.2 V are represented by equations 2 and 3. The peak positions for this thin film material (intercalation peaks: 3.38 V and 3.18 V, deintercalation peaks: 3.23 V and 3.44 V) are similar to those obtained in organic electrolytes where such well-defined peaks are typically only seen for nanostructured cathode material (intercalation peaks: 3.35 V and 3.15 V, deintercalation peaks: 3.26 V and 3.47 V).[14] The electrical conductivity for a V_2O_5 film of similar dimensions (~260 nm) film[28] is 1.17 x10^{-3} S cm^{-1} which is in the same region if not better than typical oxide materials used as cathodes for lithium ion batteries. The average lithium ion diffusion coefficient calculated for the crystalline V_2O_5 was determined to be 7.83 x10^{-10} cm^2 s^{-1} for the 220 nm films which also compares very favourably with oxide materials typically utilised.[29] The diffusion coefficients obtained for the α/ε and ε/δ phases of the film are 8.53 x10^{-10} and 7.14 x10^{-10} cm^2 s^{-1}, respectively. The sharp peaks in the voltammograms recorded at relatively high rates (0.5 mV/s over 600 mV) which approximates to a 3 C-rate also indicates the material is not

10.1002/batt.202000236

ARTICLE

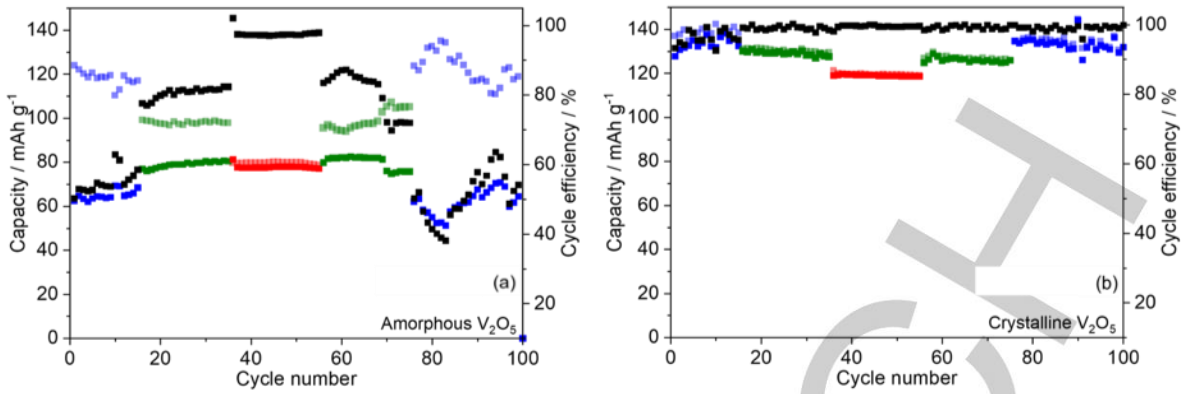

Figure 3: Comparison of electrode capacities and coulombic efficiencies (black) at various scan rates for (a) amorphous and (b) crystalline V_2O_5 thin film electrodes in 0.5 M LiTFSI in C_4mpyrTFSI. Scan rates: 0.05 mV s^{-1} (blue), 0.1 mV s^{-1} (green) and 0.5 mV s^{-1} (red).

complicated by low electronic conductivity. The current densities for the amorphous V_2O_5 are significantly lower than for the crystalline materials, which is also attributed to isotropic Li^+ diffusion pathways.[26]

The crystalline film exhibits greater capacity and cycling stability than the amorphous films during CV analysis as shown in the summary data of figure 3. The coulombic efficiency for the crystalline material is close to 100% across all scan rates investigated up to 0.5 mV/s, which is due to highly reversible Li^+ intercalation/deintercalation as evidenced by the overlapping CVs at each sweep rate in figure 2(b). The crystalline materials result in observed electrode capacities close to theoretical (147 mAh g^{-1}) for both intercalation and deintercalation (~140 mAh g^{-1} at 0.05 mV s^{-1}).

As shown in figure 3(a) the amorphous electrode exhibits low capacity and poor reversibility with significant capacity loss on cycling except at the slowest scan rate which still only achieved 80 mAh g^{-1}. This is attributed to the isotropic lithium diffusion whereby the Li^+ intercalation/deintercalation processes are not as reversible as evidenced in figure 3(b).

Galvanostatic cycling was employed to determine the rate capabilities of the amorphous and crystalline electrodes. The crystalline film exhibits the typical step profile as shown in figure 4 which is attributed to the various phase changes V_2O_5 undergoes during cycling with Li^+, while no plateau was observed in the amorphous films. The linear curves without a clearly defined plateau is indicative of pseudo-capacitor behaviour,[30] which correlates well with the CV results.

A cut-off voltage of 2.5 V was utilised due to the onset of side reactions which affected the Li intercalation/deintercalation efficiency of V_2O_5. The crystalline V_2O_5 electrode exhibits excess capacity in the initial cycles as shown in figure 4 due to the formation of a cathode electrolyte interface (CEI) layer. This results in lower coulombic efficiencies in the initial scans. Coating cathode materials with ex situ protective layers such as Al_2O_3 has been reported to yield improved electrochemical performance.[31] An alternative to such coatings is the utilisation of carbonate additives which form stable electrolyte interfaces in situ in organic solvents early on in the cycling process. VC was investigated to determine its ability to form a stable electrode/electrolyte interface in this ionic liquid-based electrolyte.

The ionic conductivity of the two electrolytes was determined by EIS at room temperature. The values for the VC-free and VC-containing electrolytes are almost identical at 1.50 and 1.54 mS cm^{-1}, respectively.

10.1002/batt.202000236

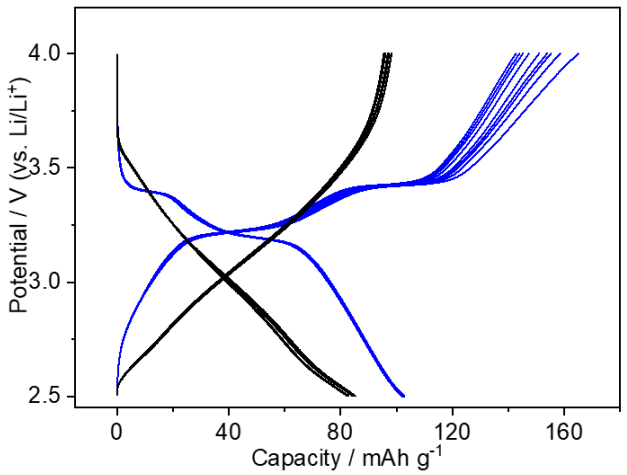

Figure 4: Galvanostatic profiles for cycles 1 to 10 for crystalline (blue) and amorphous (black) V_2O_5 thin films at 0.2 C in 0.5 M LiTFSI in C_4mpyrTFSI.

The electrode kinetics of the crystalline materials were investigated to determine if there is a change upon addition of VC to the electrolyte. Similar peak separations were obtained in the additive-free and VC-containing electrolytes across all scan rates, for example the peak separation obtained within the additive-free electrolyte was 36 and 39 mV for ε/δ and α/ε phases respectively at 0.05 mV s^{-1}, while under the same conditions, peak separations of 37 and 42 mV were observed in the VC-containing electrolyte. This indicates that the rates of Li^+ intercalation and deintercalation are similar across all scan rates. The diffusive and non-diffusive contributions (b-value) are compared for both electrolytes. The contribution from the diffusion and non-diffusion controlled kinetics can be quantified as the measured current (i) at a fixed potential (V) where the current is a combination of the two kinetic regimes, equation 4. The equation is rearranged to a line equation (equation 5) where k_1 is equal to the slope and k_2 is equal to the intercept when $\frac{i}{\sqrt{v}}$ is plotted against $\sqrt{v}$. The percentage contribution of diffusion and non-diffusion controlled kinetics is calculated using equations 6 and 7, respectively.[29, 32]

$$i = k_1 v + k_2 v^{0.5} \quad \text{Equation 4}$$

$$\frac{i}{v^{0.5}} = k_1 v^{0.5} + k_2 \quad \text{Equation 5}$$

$$\text{Diffusion controlled} = \frac{k_2 v^{0.5}}{k_1 v + k_2 v^{0.5}} \quad \text{Equation 6}$$

$$Non-diffusion\ controlled = \frac{k_1 v}{k_1 v + k_2 v^{0.5}} \quad \text{Equation 7}$$

The corresponding b values for the VC-free electrolyte and both the ε/δ and α/ε phases are ~0.75 and ~0.65, respectively. From this data it is evident that non-diffusion controlled kinetics is having an influence in the reaction as the value is higher than 0.5 which is attributed to diffusion controlled reactions solely. The non-diffusion controlled contribution increases from ~17% to ~62% as the scan rates increase from 0.05 mV s^{-1} to 0.5 mV s^{-1}. This increase is expected with phase changes as this can expose metal ions within the bulk to the outer surface and promote intercalation that is not diffusion controlled.[33] Similar b-values are obtained for the VC-containing electrolyte as shown in table 1, which indicates that the electrode kinetics are not significantly impacted by the addition of VC.

Table 1: Comparison of the peak separation between the ε/δ and α/ε phases, and b values in various electrolytes.

Scan rate (mV s^{-1})	0.5 M LiTFSI in C_4mpyrTFSI		3 wt.% VC in 0.5 M LiTFSI in C_4mpyrTFSI	
	Peak separation (mV)			
	ε/δ	α/ε	ε/δ	α/ε
0.05	36	39	37	42
0.1	54	55	50	50
0.5	132	132	131	125
b value	0.75	0.65	0.72	0.66

When the galvanostatic cycling performances of the VC-free and VC-containing electrolytes are compared, it is evident that the electrochemical performance of the crystalline material is

10.1002/batt.202000236

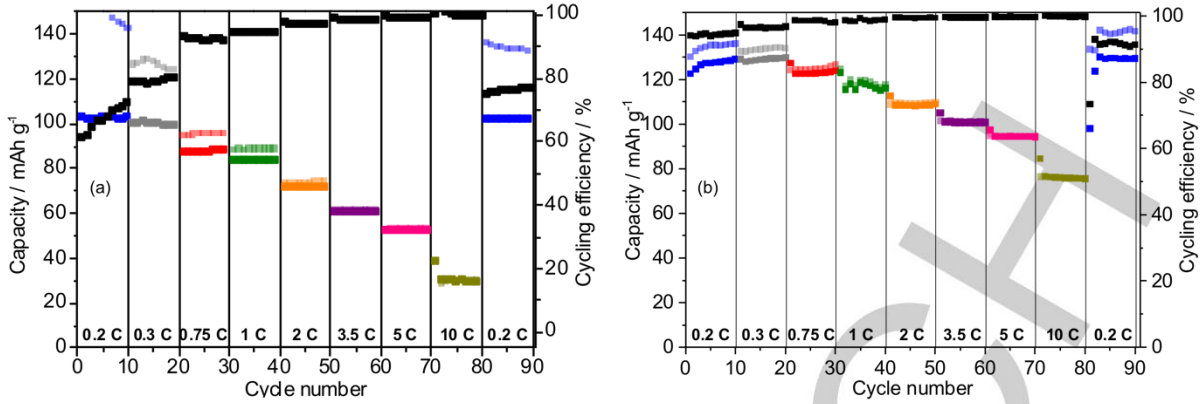

Figure 5: Comparison of crystalline electrode capacities and coulombic efficiencies (black) at various C-rates, where electrolytes used are (a) 0.5 M LiTFSI in C_4mpyrTFSI and (b) 3 wt.% VC in 0.5 M LiTFSI in C_4mpyrTFSI.

enhanced as shown in figure 5. Due to the formation of a stable interface, there is a decreased electrolyte breakdown (figure 5(b)), thus resulting in more stable cycling within VC-containing electrolytes, where higher electrode capacities (VC-free: ~90 mAh g^{-1} vs. VC-containing: ~ 120 mAh g^{-1} at 0.75 C) and coulombic efficiencies (VC-free: ~93% vs. VC-containing ~97%) are obtained.

As observed in figure 4, the amorphous electrodes yield lower electrode capacities than their crystalline counterparts in 0.5 M LiTFSI in C_4mpyrTFSI and a similar trend is observed when utilised in VC-containing electrolytes. At low rates such as 0.2 C, intercalation capacities exceed theoretical, whereby coulombic efficiencies are less than 60% which is in stark contrast with the values obtained in figure 5(b). At higher rates such as 3.5 C, the electrode capacities for the amorphous films are approximately 20 mAh g^{-1} lower than the crystalline materials (80 vs. 100 mAh g^{-1}). The crystalline material shows greater electrode capacities and better coulombic efficiencies across all C-rates when compared to the amorphous electrode in 3 wt.% VC in 0.5 M LiTFSI in C_4mpyrTFSI (5 C: 95 mAh g^{-1} and 99.7% vs. 73 mAh g^{-1} and 99%). The charge and discharge capacities of the crystalline data are 93% and 88% of the theoretical value at 0.2 C. Even at a 10 C rate the specific capacity of 52% is achieved (76 mAh g^{-1}), with a coulombic efficiency of 99.9%.

Microbatteries typically utilise a solid-state electrolyte which enables sequential layer build-up of thin film materials. Crystalline and amorphous V_2O_5 electrode were analysed with a quasi-solid-state polymer gel electrolyte containing the pyrrolidinium ionic liquid C_4mpyrTFSI, PVDF-HFP and LiTFSI salt, where C_4mpyrTFSI accounted for 60% of the mixture's weight. Once the solvent evaporated from the polymer film after solvent casting, no further post processing was required, unlike similar membranes in the literature where the polymer membrane required soaking in the electrolyte.[34] This thin film polymer gel has an ionic conductivity of 1.9 mS cm^{-1} which is comparable to the liquid analogue LiTFSI in C_4mpyrTFSI (1.5 mS cm^{-1}).[35] CV intercalation peaks at 3.39 V and 3.18 V and deintercalation peaks at 3.24 V and 3.44 V are similar to those for the liquid analogue electrolytes (intercalation peaks: 3.38 V and 3.18 V, deintercalation peaks: 3.23 V and 3.44 V). Figure 6 demonstrates the cyclability of V_2O_5 electrodes with the polymer gel of C_4mpyrTFSI, whereby the crystalline V_2O_5 exhibits higher electrode capacities than amorphous V_2O_5, 131 versus 81 mAh g^{-1} at 0.3 C, respectively. The coulombic efficiencies were above 90% for all C-rates investigated for both crystalline and amorphous materials. The electrode capacities obtained for the crystalline V_2O_5 films are similar to those obtained with 3 wt.% VC in 0.5 M C_4mpyrTFSI, and greater than those obtained in its liquid analogue 0.5 M

10.1002/batt.202000236

ARTICLE

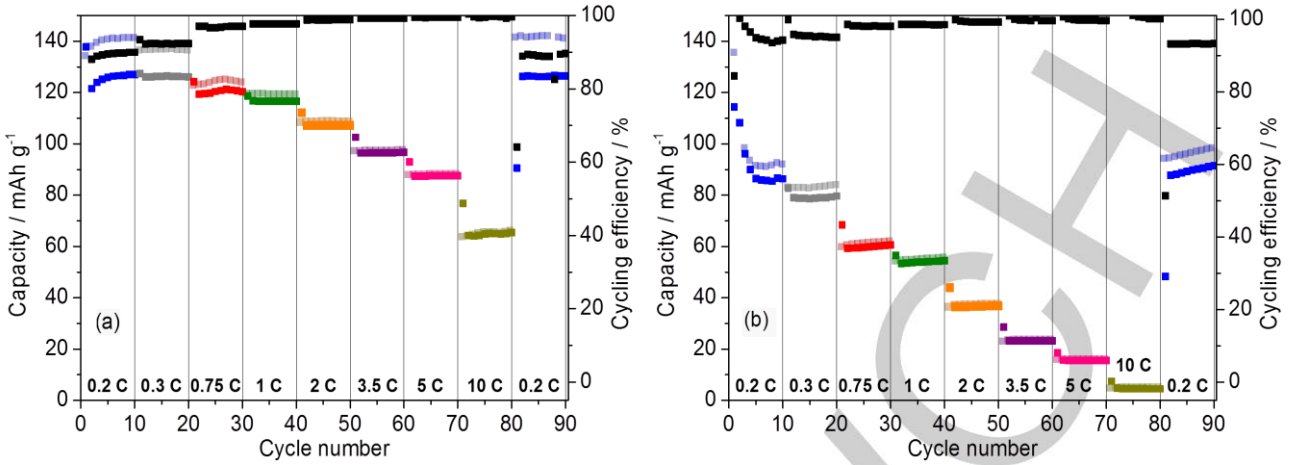

Figure 6: Comparison of electrode capacities and coulombic efficiencies (black) for (a) crystalline and (b) amorphous V_2O_5 thin films. Electrolyte: 450 µm PG-60.

LiTFSI in C_4mpyrTFSI (~120 versus ~85 mAh g^{-1} at 1 C). Again, the amorphous film exhibited poor performance with electrode capacity fading rapidly to less than half the capacity of the crystalline material at the 1 C rate.

Due to the improved electrochemical performances of the crystalline V_2O_5 electrodes with the PG-60 electrolyte and 3 wt.% VC-containing liquid electrolytes, long-term cycling was investigated. Both electrodes underwent the same initial C-rate analysis described above for figures 5 and 6, and then 50 cycles at various C-rates were analysed up to a total of 400 cycles as shown in figure 7. The crystalline V_2O_5 gave similar capacity values when cycled in the polymer gel and ionic liquid versions of the electrolyte, e.g. 110 mAh g^{-1} at 2 C. The PG-60 exhibits the better long-term cycling with minimal capacity fade (figure 7(b)), compared to the liquid electrolyte 3 wt.% VC in 0.5 M LiTFSI in C_4mpyrTFSI (0.4 vs. 2.9% over 50 cycles at 5 C). In addition, the final 0.2 C rate capacity is recovered in the PG-60 test to ~125 mAh g^{-1} after cycling at 5 C. This demonstrates that fast cycling does not lead to electrode deterioration as the final capacity matches the initial value at the 0.2 C rate. After cycling SEM, EDX and Raman analysis was carried out and compared to the results shown in figure 1. The morphological and compositional data acquired before and after cycling were identical, thus indicating no change in the films. It also indicates that lithium metal anodes can be used for long term cycling without capacity fade or short circuits developing in either the VC containing IL or the polymer gel analogue.

10.1002/batt.202000236

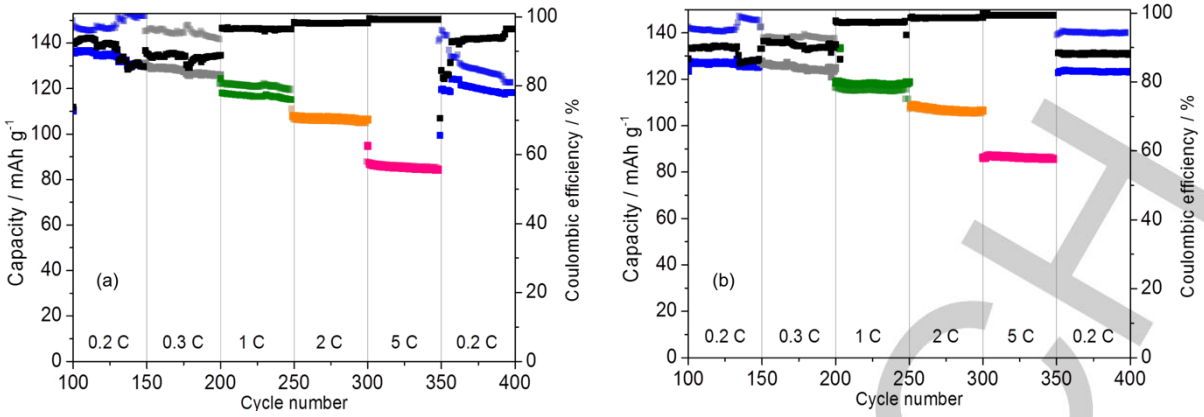

Figure 7: Comparison of electrode capacities and coulombic efficiencies (black) at various C-rates for crystalline V_2O_5 electrodes in (a) 3 wt.% VC in 0.5 M LiTFSI in C_4mpyrTFSI and (b) 450 µm PG-60

Conclusion

CV analysis of crystalline V_2O_5 yields coulombic efficiencies >99%, where high electrode capacities >120 mAh g^{-1} are obtained. This data has not been previously reported in the literature with C_4mpyrTFSI-based electrolytes. The electrodeposited V_2O_5 thin films produce sharp well-defined intercalation and deintercalation peaks in C_4mpyrTFSI, unlike the broad pseudo-capacitive-like peaks in C_3mpyrTFSI previously reported in the literature. In addition, the peak positions obtained in C_4mpyrTFSI are comparable with those obtained at nanostructured V_2O_5 in organic electrolytes demonstrating similar electrochemical performances. Utilisation of carbonate additives such as VC allow for the formation of a stable cathode electrolyte interface (CEI) layer within organic electrolytes, thus reducing the need for ex-situ protective layers such as Al_2O_3. In this work, the formation of a stable cathode electrolyte interface (CEI) layer is demonstrated with the IL, resulting in higher electrode capacities during galvanostatic cycling than for the additive free electrolyte, ~ 120 versus ~90 mAh g^{-1} at 0.75 C, without adversely affecting the electrode kinetics. These results give insight into the electrochemical performance of V_2O_5 with liquid C_4mpyr-based IL electrolytes, whereby the utilisation of suitable in situ additives reduce the need to pre-coat cathode materials with protective nanoscale layers such as Al_2O_3, which oftentimes are electrical insulators.

Crystalline V_2O_5 cycling with polymer gel electrolyte suited for layer by layer microbattery fabrication yields electrode capacities (110 mAh g^{-1} at 2 C) similar to those obtained in liquid electrolytes. Stable long-term cycling with minimal capacity fade at high C-rates is observed in the polymer gel electrolyte, for example 0.4% over 50 cycles at 5 C. In addition, the final 0.2 C rate capacity is recovered in the PG-60 test to ~125 mAh g^{-1} after cycling at 5 C. These results also indicate that lithium metal anodes can be used for long term cycling without capacity fade or short circuits developing in either the VC containing IL or the polymer gel analogue. The fabrication options described in this work for V_2O_5 with the polymer gel electrolyte and lithium metal anodes could realise all-solid-state Li microbatteries for long-life IoT sensors.

Experimental Section

Binder-free V_2O_5 was electrodeposited at room temperature using a CH Instruments 660B potentiostat onto a Si coupon with 10 nm Ti and 100 nm Au. To produce a film thickness of ~220 nm with a mass loading of 7.4 $x10^{-5}$ g, electrodeposition was carried out using a constant potential of 2 V for 10 s in a three-electrode setup with a saturated calomel electrode (SCE) and platinum (Pt) mesh as the reference and counter electrodes,

respectively. The electrochemical bath was a 0.25 M solution of $VOSO_4.xH_2O$, (assumed degree of hydration is 5) purchased from Sigma Aldrich, in a 1:1 (v/v) mixture of deionized water and ethanol.[36] After deposition, some samples were heated to 325 °C to crystallise the V_2O_5 deposit (annealed), while other samples were dried using a N_2 gun (as-deposited). The crystallinity of the samples was determined by Raman spectroscopy (Renishaw Invia, 514 nm laser).

A polymer gel electrolyte was synthesised consisting of 1-butyl-1-methylpyrrolidinium bis(trifluoromethylsulfonyl)imide (C_4mpyrTFSI), lithium bis(trifluoromethylsulfonyl) imide (LiTFSI) and PVDF-HFP as described by McGrath *et al.*[35] The polymer gels were synthesised by dissolving PVDF-HFP in molecular-sieve dried acetone at 50 °C with stirring for 30 minutes. Once dissolved, the LiTFSI was added and stirred for a further 30 minutes. Finally, C_4mpyrTFSI was added (60 wt.% of mixture) and denoted as PG-60. The mixture was stirred for 1 hour before being solvent cast into petri dishes. Once the acetone evaporated, the thickness of the polymer gel (~450 µm) was determined using a micrometre.

Electrochemical measurements of the Li^+ capacity were assessed by CV and galvanostatic cycling with potential limitation (GCPL) using a Bio-logic VSP potentiostat at various scan rates and discharge/charge currents, respectively. A three-electrode thin film pouch cell microbattery setup was utilised where 0.25 mm thick lithium foil (Sigma Aldrich) acted as counter and reference electrode. 1 cm^2 of the cathode was exposed as the working electrode to the electrolyte solutions: 0.5 M LiTFSI in C_4mpyrTFSI, 3 wt.% VC in 0.5 M LiTFSI in C_4mpyrTFSI and the polymer gel electrolyte PG-60, where 0.5 M LiTFSI was chosen as the optimum salt concentration which exhibited high ionic conductivity (1.5 mS cm^{-1}) and Li deposition and stripping capabilities. The diffusion co-efficient was determined from CV analysis using the Randle-Sevcik equation:

$$i = (2.69x10^5)n^{\frac{3}{2}}AC_{Li}D_{Li}^{\frac{1}{2}}\nu^{\frac{1}{2}} \quad \text{Equation 8}$$

Where n is the number of electrons transferred, A is the active area of the electrode, C_{Li} is the bulk concentration of Li in the electrode, and D_{Li} is the diffusion co-efficient of Li in the thin film electrode.

Cell assembly was carried out in an argon-filled glove box (M. Braun LABstar Glove Box) with O_2 and H_2O maintained below 0.1 ppm.

Acknowledgements

This publication has emanated from research supported in part by a research grant from Science Foundation Ireland (SFI) and is co-funded by the European Regional Development Fund under Grant Number 13/RC/2077 and the EU EnABLES Research Infrastructure project Powering the Internet of Things, funded by the Horizon 2020 programme under grant agreement number 730957.

Keywords: Electrodeposition, ionic liquid, lithium-ion battery, polymer gel electrolyte, vanadium oxide, lithium metal, vinylene carbonate

[1] Statista, in *Consumer Electronics*, https://www.statista.com/statistics/471264/iot-number-of-connected-devices-worldwide/, **2016**.

[2] P. Barrera, Top Cobalt Reserves by Country. https://investingnews.com/daily/resource-investing/battery-metals-investing/cobalt-investing/cobalt-producer-cobalt-reserves/, **2019**.

[3] Trading Economics, Cobalt 2010-2020 Data. https://tradingeconomics.com/commodity/cobalt, **2020**.

[4] aD. Liu, Y. Liu, B. B. Garcia, Q. Zhang, A. Pan, Y. H. Jeong, G. Cao, *Journal of Materials Chemistry* **2009**, *19*, 8789-8795; bD. Yu, C. Chen, S. Xie, Y. Liu, K. Park, X. Zhou, Q. Zhang, J. Li, G. Cao, *Energy and Environmental Science* **2011**, *4*, 858-861; cY. Shimizu, K. Nagase, N. Miura, N. Yamazoe, *Solid State Ionics* **1992**, *53-56*, 490-495.

[5] aA. A. Akl, *J Phys Chem Solids* **2010**, *71*, 223-229; bA. Bouzidi, N. Benramdane, A. Nakrela, C. Mathieu, B. Khelifa, R. Desfeux, A. Da Costa, *Materials Science and Engineering: B* **2002**, *95*, 141-147; cL. Boudaoud, N. Benramdane, R. Desfeux, B. Khelifa, C. Mathieu, *Catalysis Today* **2006**, *113*, 230-234.

[6] aX. Wu, F. Lai, L. Lin, Y. Li, L. Lin, Y. Qu, Z. Huang, *Applied Surface Science* **2008**, *255*, 2840-2844; bK.-C. Cheng, F.-R. Chen, J.-J. Kai, *Solar Energy Materials and Solar Cells* **2006**, *90*, 1156-1165.

[7] aC. V. Ramana, O. M. Hussain, B. S. Naidu, C. Julien, M. Balkanski, *Mater. Sci. Eng. B* **1998**, *52*, 32-39; bC. V. Ramana, O. M. Hussain, B. S. Naidu, *Materials Chemistry and Physics* **1997**, *50*, 195-199.

[8] aR. Teghil, L. D'Alessio, A. De Bonis, A. Galasso, N. Ibris, A. M. Salvi, A. Santagata, P. Villani, *J Phys Chem A* **2009**, *113*, 14969-

14974; bC. Julien, E. Haro-Poniatowski, M. A. Camacho-López, L. Escobar-Alarcón, J. Jímenez-Jarquín, *Materials Science and Engineering: B* **1999**, *65*, 170-176.

[9] aH. Groult, K. Le Van, A. Mantoux, L. Perrigaud, P. Doppelt, *Journal of Power Sources* **2007**, *174*, 312-320; bN. Thi Be Bay, P. M. Tien, S. Badilescu, Y. Djaoued, G. Bader, F. E. Girouard, V. v. Truong, L. q. Nguyen, *Journal of Applied Physics* **1996**, *80*, 7041-7045.

[10] T. Gallasch, T. Stockhoff, D. Baither, G. Schmitz, *Journal of Power Sources* **2011**, *196*, 428-435.

[11] aY.-R. Lu, T.-Z. Wu, C.-L. Chen, D.-H. Wei, J.-L. Chen, W.-C. Chou, C.-L. Dong, *Nanoscale research letters* **2015**, *10*, 387-387; bA. M. Engstrom, F. M. Doyle, *Journal of Power Sources* **2013**, *228*, 120-131; cD. Rehnlund, M. Valvo, K. Edström, L. Nyholm, *Journal of The Electrochemical Society* **2014**, *161*, D515-D521; dM. Rasoulis, D. Vernardou, *Coatings* **2017**, *7*; eE. Armstrong, M. O'Sullivan, J. O'Connell, J. D. Holmes, C. O'Dwyer, *Journal of The Electrochemical Society* **2015**, *162*, D605-D612.

[12] aH. Poelman, H. Tomaszewski, D. Poelman, L. Fiermans, R. D. Gryse, M. F. Reyniers, G. B. Marin, *Surface and Interface Analysis* **2002**, *34*, 724-727; bY. S. Yoon, J. S. Kim, S. H. Choi, *Thin Solid Films* **2004**, *460*, 41-47.

[13] aC. Delmas, H. Cognac-Auradou, J. M. Cocciantelli, M. Ménétrier, J. P. Doumerc, *Solid State Ionics* **1994**, *69*, 257-264; bD. Acosta, A. Perez, C. Magaña, F. Hernandez, *Journal of Materials Science and Engineering A* **2016**, *6*; cC. R. Aita, L.-J. Liou, C.-K. Kwok, R. C. Lee, E. Kolawa, *Thin Solid Films* **1990**, *193-194*, 18-26; dI. Quinzeni, S. Ferrari, E. Quartarone, P. Mustarelli, *Journal of Power Sources* **2011**, *196*, 10228-10233; eL. Ottaviano, A. Pennisi, F. Simone, A. M. Salvi, *Optical Materials* **2004**, *27*, 307-313; fH. M. R. Giannetta, C. Calaza, D. G. Lamas, L. Fonseca, L. Fraigi, *Thin Solid Films* **2015**, *589*, 730-734; gM. Panagopoulou, D. Vernardou, E. Koudoumas, D. Tsoukalas, Y. S. Raptis, *Electrochimica Acta* **2017**, *232*, 54-63.

[14] Y. L. Cheah, V. Aravindan, S. Madhavi, *ACS Applied Materials & Interfaces* **2013**, *5*, 3475-3480.

[15] J. F. M. Oudenhoven, L. Baggetto, P. H. L. Notten, *Advanced Energy Materials* **2011**, *1*, 10-33.

[16] S.-L. Chou, J.-Z. Wang, J.-Z. Sun, D. Wexler, M. Forsyth, H.-K. Liu, D. R. MacFarlane, S.-X. Dou, *Chemistry of Materials* **2008**, *20*, 7044-7051.

[17] aG. A. Elia, U. Ulissi, S. Jeong, S. Passerini, J. Hassoun, *Energy & Environmental Science* **2016**, *9*, 3210-3220; bD. Di Lecce, J. Hassoun, *ACS Omega* **2018**, *3*, 8583-8588.

[18] H.-T. Fang, M. Liu, D.-W. Wang, T. Sun, D.-S. Guan, F. Li, J. Zhou, T.-K. Sham, H.-M. Cheng, *Nanotechnology* **2009**, *20*, 225701.

[19] aH. Ota, K. Shima, M. Ue, J.-i. Yamaki, *Electrochimica Acta* **2004**, *49*, 565-572; bZ. Peng, X. Cao, P. Gao, H. Jia, X. Ren, S. Roy, Z. Li, Y. Zhu, W. Xie, D. Liu, Q. Li, D. Wang, W. Xu, J.-G. Zhang, *Advanced Functional Materials* **2020**, *30*, 2001285.

[20] B. Pandit, D. P. Dubal, P. Gómez-Romero, B. B. Kale, B. R. Sankapal, *Scientific Reports* **2017**, *7*, 43430.

[21] aS. Liu, Z. Tong, J. Zhao, X. Liu, J. wang, X. Ma, C. Chi, Y. Yang, X. Liu, Y. Li, *Physical Chemistry Chemical Physics* **2016**, *18*, 25645-25654; bC. Sanchez, J. Livage, G. Lucazeau, *Journal of Raman Spectroscopy* **1982**, *12*, 68-72; cH. Drosos, A. Sapountzis, E. Koudoumas, N. Katsarakis, D. Vernardou, *Journal of The Electrochemical Society* **2012**, *159*, E145-E147; dS.-H. Lee, H. M. Cheong, M. J. Seong, P. Liu, C. E. Tracy, A. Mascarenhas, J. R. Pitts, S. K. Deb, *Solid State Ionics* **2003**, *165*, 111-116; eP. Shvets, O. Dikaya, K. Maksimova, A. Goikhman, *Journal of Raman Spectroscopy* **2019**, *50*, 1226-1244; fS.-H. Lee, H. M. Cheong, M. J. Seong, P. Liu, C. E. Tracy, A. Mascarenhas, J. R. Pitts, S. K. Deb, *Journal of Applied Physics* **2002**, *92*, 1893-1897.

[22] aR. Baddour-Hadjean, J. P. Pereira-Ramos, C. Navone, M. Smirnov, *Chemistry of Materials* **2008**, *20*, 1916-1923; bR. Baddour-Hadjean, A. Marzouk, J. P. Pereira-Ramos, *Journal of Raman Spectroscopy* **2012**, *43*, 153-160.

[23] aL. Abello, E. Husson, Y. Repelin, G. Lucazeau, *Spectrochimica Acta Part A: Molecular Spectroscopy* **1983**, *39*, 641-651; bJ. M. Jehng, F. D. Hardcastle, I. E. Wachs, *Solid State Ionics* **1989**, *32-33*, 904-910.

[24] A. Ghosh, E. J. Ra, M. Jin, H.-K. Jeong, T. H. Kim, C. Biswas, Y. H. Lee, *Advanced Functional Materials* **2011**, *21*, 2541-2547.

[25] aJ. B. Bates, N. J. Dudney, G. R. Gruzalski, R. A. Zuhr, A. Choudhury, C. F. Luck, J. D. Robertson, *Journal of Power Sources* **1993**, *43*, 103-110; bE. Uchaker, Y. Z. Zheng, S. Li, S. L. Candelaria, S. Hu, G. Z. Cao, *Journal of Materials Chemistry A* **2014**, *2*, 18208-18214.

[26] aC. Julien, G.-A. Nazri, in *Solid State Batteries: Materials Design and Optimization*, Springer US, Boston, MA, **1994**, pp. 1-96; bF. Mattelaer, K. Geryl, G. Rampelberg, J. Dendooven, C.

Detavernier, *ACS Applied Materials & Interfaces* **2017**, *9*, 13121-13131.

[27] aX. Liu, J. Zeng, H. Yang, K. Zhou, D. Pan, *RSC Advances* **2018**, *8*, 4014-4031; bX. Zhang, J.-G. Wang, H. Liu, H. Liu, B. Wei, *Materials (Basel, Switzerland)* **2017**, *10*, 77.

[28] J. C. Badot, A. Mantoux, N. Baffier, O. Dubrunfaut, D. Lincot, *Journal of Materials Chemistry* **2004**, *14*, 3411-3415.

[29] T. M. Clancy, J. F. Rohan, *ChemElectroChem* **2018**, *5*, 3273-3278.

[30] E. Brown, S.-H. Park, A. Elangovan, Y. Yuan, J. Kim, X. S. Sun, X. Zhang, G. Wang, J. Li, *Electrochimica Acta* **2018**, *269*, 144-154.

[31] aT. Teranishi, Y. Yoshikawa, M. Yoneda, A. Kishimoto, J. Halpin, S. O'Brien, M. Modreanu, I. M. Povey, *ACS Applied Energy Materials* **2018**, *1*, 3277-3282; bP. Yan, J. Zheng, X. Zhang, R. Xu, K. Amine, J. Xiao, J.-G. Zhang, C.-M. Wang, *Chemistry of Materials* **2016**, *28*, 857-863.

[32] S. Gong, G. Zhao, P. Lyu, K. Sun, *Journal of Materials Chemistry A* **2019**, *7*, 1187-1195.

[33] Y. Wang, Y. Song, Y. Xia, *Chemical Society Reviews* **2016**, *45*, 5925-5950.

[34] J.-K. Kim, L. Niedzicki, J. Scheers, C.-R. Shin, D.-H. Lim, W. Wieczorek, P. Johansson, J.-H. Ahn, A. Matic, P. Jacobsson, *Journal of Power Sources* **2013**, *224*, 93-98.

[35] L. M. McGrath, J. Jones, E. Carey, J. F. Rohan, *ChemistryOpen* **2019**, *8*, 1429-1436.

[36] E. Armstrong, D. McNulty, H. Geaney, C. O'Dwyer, *ACS Applied Materials & Interfaces* **2015**, *7*, 27006-27015.